LINKING GAS FRACTIONS TO BIMODALITIES IN GALAXY PROPERTIES

SHEILA J. KANNAPPAN[1]
Accepted to ApJL

ABSTRACT

Galaxies over four decades in stellar mass are shown to obey a strong correlation between $u-K$ colors and atomic-gas-to-stellar mass ratios (G/S), using stellar mass-to-light ratios derived from optical colors. The correlation holds for G/S ranging from nearly 10:1 to 1:100 for a sample obtained by merging the SDSS DR2, 2MASS, and HYPERLEDA H I catalogs. This result implies that $u-K$ colors can be calibrated to provide "photometric gas fractions" for statistical applications. Here this technique is applied to a sample of $\sim$35,000 SDSS-2MASS galaxies to examine the relationship of gas fractions to observed bimodalities in galaxy properties as a function of color and stellar mass. The recently identified transition in galaxy properties at stellar masses ~ 2–3×10^{10} M$_\odot$ corresponds to a shift in gas richness, dividing low-mass late-type galaxies with G/S $\sim$ 1:1 from high-mass galaxies with intermediate-to-low G/S. Early-type galaxies below the transition mass also show elevated G/S, consistent with formation scenarios involving mergers of low-mass gas-rich systems and/or cold-mode gas accretion.

Subject headings: galaxies: evolution

1. INTRODUCTION

Analyses of galaxies in the Sloan Digital Sky Survey (SDSS) have demonstrated two distinct bimodalities in galaxy properties: a bimodality between recent-burst dominated and more continuous star formation histories (SFHs) as a function of stellar mass M_*, divided at $M_* \sim 3 \times 10^{10}$ M$_\odot$ (Kauffmann et al. 2003b), and a bimodality between blue late-type and red early-type galaxy sequences as a function of optical color, divided at $u-r \sim 2.2$ (Strateva et al. 2001; Hogg et al. 2002; Blanton et al. 2003b). Recently, Baldry et al. (2004) have partially unified these observations, demonstrating a color transition within each of the two galaxy sequences at $M_* \sim 2 \times 10^{10}$ M$_\odot$, as well as an increase in the relative number density of red sequence galaxies above $\sim$2–5$\times 10^{10}$ M$_\odot$. They also argue that the number density of the red sequence is consistent with a major-merger origin. However, the cause of the color and SFH transitions at $\sim$2–3$\times 10^{10}$ M$_\odot$ remains to be explained.

Several physical processes that influence SFHs may imprint a transition mass on the galaxy population. Supernova-driven gas blow-away will preferentially affect halos with small escape velocities (Dekel & Silk 1986), although simulations suggest that the baryonic mass threshold for blow-away may be closer to 10^7 M$_\odot$ than to 10^{10} M$_\odot$ (Mac Low & Ferrara 1999). Cold-mode gas accretion may dominate in low-mass halos whose gas fails to shock to the virial temperature (Birnboim & Dekel 2003; Katz et al. 2003); here analytic estimates give a threshold mass of a few times 10^{11} M$_\odot$ including dark matter, so a link to the observed transition at $M_* \sim 2$–3×10^{10} M$_\odot$ is plausible. Finally, observations suggest that inefficient star formation may be typical of disk-dominated galaxies with $V_c \lesssim 120$km s^{-1}, possibly reflecting the relative importance of supernova feedback as opposed to other turbulence drivers in supporting the interstellar medium against gravitational instability (Dalcanton et al. 2004).

All of these processes involve gas – its expulsion, accretion, or rate of consumption. Thus examining how the gas properties of galaxies vary with color and stellar mass may offer vital clues to the origin of the transition mass and the color shifts within the red and blue sequences. Unfortunately, tracing the dominant neutral phase of the interstellar medium requires H I 21-cm line observations, which are challenging even at the modest redshifts probed by the SDSS. To make full use of the statistical power of the SDSS, an alternate strategy is required.

Building on earlier optical work (e.g., Roberts 1969), Bothun (1984) has shown a remarkably tight correlation between H I mass-to-H-band luminosity ratios and $B-H$ colors. Going one step further, the present work describes a method for estimating atomic-gas-to-stellar mass ratios using $u-K$ colors from the SDSS and Two Micron All Sky Survey (2MASS) databases. This "photometric gas fraction" technique is calibrated using H I data from the recently expanded HYPERLEDA H I catalog. When the technique is applied to a sample of $\sim$35,000 SDSS-2MASS galaxies at $z < 0.1$, the transition mass of 2–3$\times 10^{10}$ M$_\odot$ is observed to correspond to a shift in gas richness found separately in both galaxy color sequences. This result implies that any explanation of the transition mass via gas physics must directly or indirectly affect both early- and late-type galaxies.

2. DATA

Optical, near-IR, and H I data were obtained from the SDSS second data release (DR2, Abazajian et al. 2004), the 2MASS all-sky extended source catalog (XSC, Jarrett et al. 2000), and the HYPERLEDA homogenized H I catalog (Paturel et al. 2003). Merged catalogs were constructed containing all $z < 0.1$, $r < 17.77$, $K < 15$ galaxies with positions matched to within $6''$ and with reliable redshifts and magnitudes based on data flags and cataloged errors (magnitude errors < 0.3 in K, < 0.4 in H I, and < 0.15 in ugr). The 2MASS magnitude limit was set fainter than the completeness limit to improve statistics on dwarf and low surface brightness galaxies. As the 2MASS XSC has uneven depth, it probes significantly fainter than the completeness limit in some areas of the sky. Because of their marginal detectability, galaxies with H I-derived gas-to-stellar mass ratios greater than two were targeted for individual inspection, and eight were rejected as having unreliable 2MASS or SDSS pipeline reductions. These rejections exacerbate the shortage of IR-faint galaxies. The final samples are: SDSS-HYPERLEDA (575 galaxies), SDSS-2MASS-HYPERLEDA (346 galaxies), and SDSS-2MASS (35,166 galaxies). An additional requirement for the SDSS-2MASS sample was that the Local Group

[1] Harlan Smith Fellow, McDonald Observatory, The University of Texas at Austin, 1 University Station C1402, Austin, TX 78712-0259; sheila@astro.as.utexas.edu

motion-corrected redshift be greater than 1000 km s^{-1}.

All optical and IR magnitudes used here are fitted magnitudes, i.e. SDSS model magnitudes and 2MASS extrapolated total magnitudes. The SDSS magnitudes are corrected for Galactic extinction using the DR2 tabulated values and k-corrected to redshift zero using **kcorrect v3.2** (Blanton et al. 2003a), while the 2MASS K-band magnitudes are k-corrected using $k(z) = -2.1z$ (Bell et al. 2003). Distances are computed in the concordance cosmology $\Omega_m = 0.3$, $\Omega_\Lambda = 0.7$, $H_0 = 70$ km s^{-1} Mpc^{-1}.

3. RESULTS

Fig. 1a shows the basic correlation between u-band and 21-cm apparent magnitudes m_u and m_{HI} for the SDSS-HYPERLEDA sample. Its existence is not surprising: u-band light is a tracer of young massive stars, and the birth rate of young stars is known to depend on the available gas reservoir (as in the global correlation between disk-averaged star formation rate and gas surface density, Kennicutt 1989). The presence of young massive stars may also enhance H I detection (e.g., Shaya & Federman 1987). The absolute magnitude correlation obtained by distance-correcting m_u and m_{HI} is of course far stronger than the correlation in Fig. 1a, but at the cost of non-independent axes. In any case, what is relevant for predicting m_{HI} from m_u is not correlation strength but scatter. Most of the 0.92 mag scatter in the m_u–m_{HI} relation is not explained by the errors. This scatter likely represents variations in u-band extinction, molecular-to-atomic gas ratios, and the physical conditions required to convert a gas reservoir into young stars. Even without calibrating these factors, the m_u–m_{HI} relation is sufficiently tight for the present application.

Figs. 1b and 1c plot atomic-gas-to-stellar mass ratios (G/S) against $u-r$ and $u-K$ colors for the SDSS-2MASS-HYPERLEDA sample. Gas masses are derived from H I fluxes with a helium correction factor of 1.4, and stellar masses are derived from K-band fluxes using stellar mass-to-light (M/L) ratios estimated from $g-r$ colors as in Bell et al. (2003). The resulting correlations are distance-independent and extremely strong, with Spearman rank correlation coefficients of 0.75 and 0.69 for $u-K$ and $u-r$ respectively. Note that the calibration sample spans the color–M_* relation (Fig. 2a), and the color–G/S relation is tighter than the color–M_* relation for these galaxies by $\sim$25% in both $u-K$ and $u-r$. The strength of the $u-K$ color–G/S relation derives both from the underlying m_u–m_{HI} relation and from the close correspondence between K-band light and stellar mass. The latter correspondence is assumed within this work and may not apply to all starbursting systems (Pérez-González et al. 2003); however, Kauffmann et al. (2003a) find that spectroscopically determined M/L ratios generally agree well with color-based M/L ratios, even in the low-mass regime where starbursts are common.

The large dynamic range of the $u-K$ color–G/S relation makes the relation forgiving of errors and thus well-suited to low-precision estimation of photometric gas fractions. The 0.37 dex scatter in the relation provides a basis for error estimation. Furthermore, galaxies of low and high mass define broadly similar $u-K$ color–G/S relations in their regime of overlap (triangles and dots in Fig. 1c). It should be borne in mind that the generality of the photometric gas fraction technique as currently formulated relies on the fact that heavily dust-enshrouded star formation, as in luminous infrared galaxies, is rare in the low-z universe (Sanders & Mirabel 1996). In dusty systems one might find high G/S linked to red $u-K$ colors. Also, the

calibration given here could significantly underestimate actual gas-to-stellar mass ratios if stellar M/L ratios are much lower than assumed and/or molecular gas corrections are large (a controversial topic; see Casoli et al. 1998; Boselli et al. 2002). The M/L ratios used here are roughly consistent with maximum disk assumptions for spiral galaxies (Bell et al. 2003). Within the $ugriz$ magnitude set, the best alternative to the $u-K$ color–G/S relation is the $u-r$ color–G/S relation. Its larger scatter may in part reflect the fact that K-band magnitude errors will move points along the $u-K$ color–G/S relation, but away from the $u-r$ color–G/S relation. However, the effect from cataloged errors is quite small (arrows in Figs. 1b and 1c), so the greater $u-r$ scatter seems to be mostly physical.

Fig. 2a plots $u-r$ color vs. M_* for the $\sim$35,000-galaxy SDSS-2MASS sample, with points color-coded to indicate photometric gas fractions G/S$_{phot}$ (computed from $u-K$ colors and the fit in Fig. 1c). The well-known red and blue sequences (referring to galaxy color, not color-coding) are roughly separated by the dashed line (an approximation to the separator of Baldry et al. 2004). Within each sequence, the color-coding reveals a shift in gas fractions near a threshold mass of $M_*^t \sim 1$–3×10^{10} M$_\odot$. Massive red-sequence galaxies are extremely gas-poor (G/S$_{phot}$ as low as 1:100, red/yellow color-coded points), whereas for red-sequence galaxies below M_*^t, intermediate gas fractions (G/S$_{phot} \sim 1:10$, green points) are the norm. Likewise, massive blue-sequence galaxies have intermediate gas fractions (G/S$_{phot} \sim 1:10$, green points), but blue-sequence galaxies below M_*^t are typically gas rich (G/S$_{phot} \sim 1:1$, blue points).

These results are shown in binned form in Fig. 2b, where the contours show the conditional probability distribution of $u-r$ on M_*. In this plot, a vertical slice through the contours at a given mass gives the one-dimensional probability distribution for $u-r$ colors at that mass. The conditional probability distribution is formed by weighting each galaxy by $1/V_{max}$, where V_{max} is the maximum volume within which it could have been detected, then normalizing the counts in each color×mass bin by the total counts in each mass column. Bins with fewer than four galaxies are not considered. This algorithm is most robustly applied to truly magnitude-limited samples, but the results shown here look qualitatively similar to those of Baldry et al. (2004) for a magnitude-limited SDSS sample. Each galaxy is assigned the smallest of three V_{max} estimates, based on (i) the magnitude limit in r, (ii) the magnitude limit in K, and (iii) the distance limit imposed by the $z < 0.1$ selection requirement.

The color-coded symbols in Fig. 2b illustrate gas fraction and morphology trends using $1/V_{max}$-weighted bin averages. Ovals and S-shapes identify early and late type morphologies, respectively, based on the concentration index C_r (defined as r_{90}/r_{50}, where r_{90} and r_{50} are the 90% and 50% Petrosian radii). A value of $C_r = 2.6$ is commonly used to divide early and late types when true morphological type information is lacking (Strateva et al. 2001; Kauffmann et al. 2003a; Bell et al. 2003). Fig. 2b indicates transitional values ($2.55 < C_r < 2.65$) with both type symbols. Some of the bluest low-mass galaxy bins show transitional types, which will not be examined here. Otherwise, the blue sequence forms a broad, low C_r strip, with a shift in gas richness at $M_*^t \sim 1$–3×10^{10} M$_\odot$. At a similar mass, the red sequence shows a coordinated shift in gas richness and C_r.

Intriguingly, the increased gas content of the red sequence below M_*^t causes the red and blue sequences to fuse (nearly) in a plot of G/S$_{phot}$ vs. M_* (Fig. 2c). The double-peaked, slightly S-shaped contours of the G/S$_{phot}$ vs. M_* distribution thus look
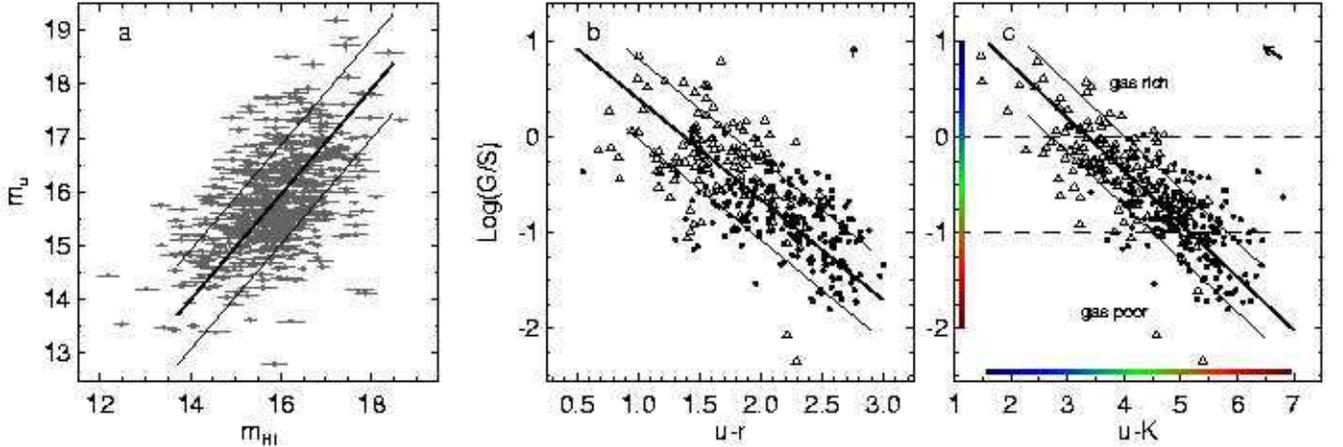
FIG. 1.— (a) Apparent u-band magnitude vs. apparent H I magnitude for the SDSS-HYPERLEDA sample. A bisector fit yields $m_u = 0.33 + 0.98 m_{HI}$ (thick line) with $\sigma = 0.92$ mag (thin lines). (b and c) Atomic-gas-to-stellar mass ratio G/S vs. $u-r$ and $u-K$ color for the SDSS-2MASS-HYPERLEDA sample. Bisector fits yield $\log(G/S) = 1.46 - 1.06(u-r)$ and $\log(G/S) = 1.87 - 0.56(u-K)$ (thick lines) with $\sigma = 0.42$ dex and 0.37 dex, respectively (thin lines). Arrows indicate the effect of a 0.3 mag error in K (the maximum allowed by selection). *The color bar in panel c provides a key to the photometric gas fractions in Fig. 2.* Horizontal lines demarcate gas-rich, intermediate, and gas-poor regimes. Dots and triangles mark galaxies with M_* above and below 2×10^{10} M$_\odot$, respectively.
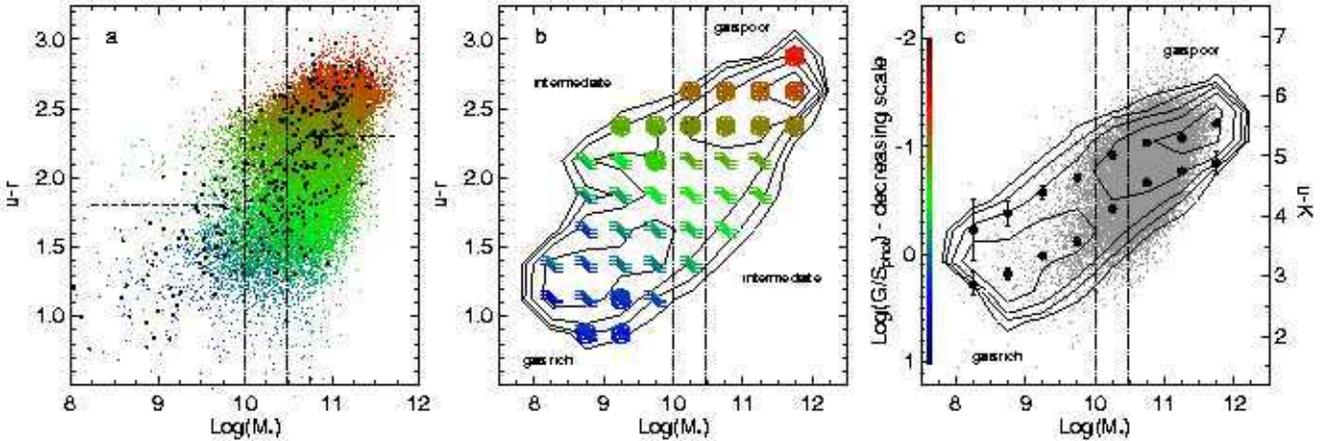

FIG. 2.— Galaxy color vs. stellar mass for the SDSS-2MASS sample. Vertical lines show the transition mass interval at 1–3×10^{10} M$_\odot$. (a) Individual $u-r$ data points color-coded by photometric gas fraction G/S$_{phot}$ (computed using $u-K$). The dashed line divides the red and blue sequences (referring to galaxy color, not color-coding), approximating the optimal divider of Baldry et al. (2004). The natural separation of the sequences is clearest in the high-resolution online figure. Black dots show the H I calibration sample of Figs. 1b and c. (b) Gas fraction and morphology trends within the red and blue sequences. Contours show the conditional probability distribution of $u-r$ on M_*, in bins of 0.25×0.5 in color$\times\log(M_*)$. Each galaxy is inverse-volume-weighted (see text) and all bins of a given mass are normalized by the total for that mass column. Each bin has three slightly offset symbols whose colors show the weighted mean and $\pm 1\sigma$ values of G/S$_{phot}$, with errors propagated from the scatter in the $u-K$ color–G/S relation. Ovals and S-shapes indicate early and late type bins based on weighted mean concentration index (see text). (c) G/S$_{phot}$ (or equivalently $u-K$) vs. stellar mass. Small points show individual values, while contours give the conditional probability distribution of G/S$_{phot}$ and $u-K$ on M_*, in bins of 0.5×0.5 in color$\times\log(M_*)$. Large points show weighted mean G/S$_{phot}$ trends for the red and blue sequences separately, using the $u-r$ division in panel a. All contours start at 0.04 and increase by $10^{0.25}\times$ at each step.

qualitatively similar to the bimodal distribution of SFH vs. M_* reported by Kauffmann et al. (2003b).[2] This similarity suggests that the bimodality in SFHs may be intimately related to changes in G/S. The contours in Fig. 2c show a broad shift near $\sim 10^{10}$ M$_\odot$, while the individual trends in the red and blue sequences change slope over the range ~ 1–3×10^{10} M$_\odot$ (though the latter changes are not independent of the method of separating the two sequences). Kauffmann et al. find a single-sequence bimodal structure in C_r vs. M_* as well, perhaps because of the decreasing C_r of the red sequence below M_*^t.

Despite low C_r values and high gas contents, the low-mass red sequence does fit into the general merger scenario for the origin of early-type galaxies, in a way that may illuminate the

Kauffmann et al. results. The low-mass red sequence maps closely to an abundant population of faint, moderately gas-rich S0 and S0/a galaxies observed in the Nearby Field Galaxy Survey, a survey designed to represent the natural distribution of galaxy types over a wide range of luminosities (Jansen et al. 2000; Kannappan et al. 2002, see Fig. 3 of the latter). Based on the frequency of gas-stellar counterrotation in this population and the scarcity of dwarf intermediate-type spiral galaxies, Kannappan & Fabricant (2001) argue that $\gtrsim 50\%$ of low-luminosity S0's may form via late-type dwarf mergers. Such gas-rich mergers would naturally produce remnants with modest C_r, explaining why low-luminosity early types are predominantly S0 rather than E galaxies. Moreover, low-luminosity

---

[2] Note that the bimodalities in question are bimodalities in the conditional probability distribution and need not appear directly in the observed galaxy distribution.

S0's quite often have blue, starbursting centers, despite red outer disks (Tully et al. 1996; Jansen et al. 2000), and such color gradients correlate with evidence of *recent* interactions (in all morphological types, Kannappan et al. 2004). The SFH measures adopted by Kauffmann et al. (2003b), which are based on $3''$-aperture spectroscopy, may emphasize the starbursting centers of this class of galaxies (and conversely, the quiescent bulges of many high-mass late-type systems), reinforcing the single-sequence structure of the resulting SFH vs. M_* plots.

4. DISCUSSION

A connection between star formation histories and gas fractions is in some sense obvious: gas must be consumed to form stars, so old red stellar populations will tend to be associated with diminished gas supplies. However, galaxies also accrete and expel gas, so this simple view misses much of the story. A complete picture must explain why gas fractions depend on mass, and in particular why there is such a close coincidence between the transition to gas richness (atomic-gas-to-stellar mass ratio $\sim$ 1:1 in the blue sequence) and the shift to recent-burst dominated SFHs below ~ 2–$3 \times 10^{10}\,M_\odot$. Critical transition masses are predicted by scenarios involving starburst-driven gas blow-away, inefficient star formation below a gravitational instability threshold, and/or cold-mode gas accretion (Dekel & Silk 1986; Verde et al. 2002; Birnboim & Dekel 2003; Katz et al. 2003; Dalcanton et al. 2004). The abundance of gas in low-mass (10^8–$10^{10}\,M_\odot$) galaxies seen in this paper is hard to explain if global gas blow-away is a dominant process in this mass regime. However, localized gas blowout or strong feedback could inhibit efficient widespread star formation in low-mass disk galaxies. Such scenarios would not explicitly account for the gas in low-mass red-sequence galaxies, but formation via mergers of low-mass late-type systems, as discussed above, could allow low-mass red-sequence galaxies to acquire their modest gas excesses from gas-rich progenitors and thereby inherit the progenitors' threshold mass for increased gas fractions. Alternatively, it is possible that the transition in star formation modes at ~ 2–$3 \times 10^{10}\,M_\odot$ is not a cause, but an *effect* of changing gas fractions, as in cold-mode accretion scenarios. If so, low-mass galaxies may form stars reasonably efficiently and still appear gas rich. The excess gas in low-mass red-sequence galaxies could in this case represent post-merger cold-mode accretion, possibly as part of a process of disk regrowth.

In conclusion, this paper has demonstrated a shift in galaxy gas mass fractions at $M_*^t \sim 1$–$3 \times 10^{10}\,M_\odot$, likely related to the shift in SFHs observed near the same stellar mass by Kauffmann et al. (2003b). The link may be causal in either direction, depending on the relative importance of supernova blowout, feedback, and cold-mode accretion processes in determining M_*^t. To establish this result, a technique has been introduced to estimate photometric gas fractions based on the correlation between $u-K$ colors and atomic-gas-to-stellar mass ratios. This correlation is interesting in its own right (see also Bothun 1984) and will be further examined and applied in future work.

REFERENCES

Abazajian, K. et al. 2004, preprint (astro-ph/0403325)
Baldry, I. K., Glazebrook, K., Brinkmann, J., Ivezić, Ž., Lupton, R. H., Nichol, R. C., & Szalay, A. S. 2004, ApJ, 600, 681
Bell, E. F., McIntosh, D. H., Katz, N., & Weinberg, M. D. 2003, ApJS, 149, 289
Birnboim, Y. & Dekel, A. 2003, MNRAS, 345, 349
Blanton, M. R., et al. 2003a, AJ, 125, 2348
Blanton, M. R., et al. 2003b, ApJ, 594, 186
Boselli, A., Lequeux, J., & Gavazzi, G. 2002, A&A, 384, 33
Bothun, G. D. 1984, ApJ, 277, 532
Casoli, F., et al. 1998, A&A, 331, 451
Dalcanton, J. J., Yoachim, P., & Bernstein, R. A. 2004, ApJ, 608, 189
Dekel, A. & Silk, J. 1986, ApJ, 303, 39
Hogg, D. W., et al. 2002, AJ, 124, 646
Jansen, R. A., Franx, M., Fabricant, D., & Caldwell, N. 2000, ApJS, 126, 271
Jarrett, T. H., Chester, T., Cutri, R., Schneider, S., Skrutskie, M., & Huchra, J. P. 2000, AJ, 119, 2498
Kannappan, S. J. & Fabricant, D. G. 2001, AJ, 121, 140
Kannappan, S. J., Fabricant, D. G., & Franx, M. 2002, AJ, 123, 2358
Kannappan, S. J., Jansen, R. A., & Barton, E. J. 2004, AJ, 127, 1371
Katz, N., Keres, D., Dave, R., & Weinberg, D. H. 2003, in ASSL Vol. 281: The IGM/Galaxy Connection. The Distribution of Baryons at z=0, 185
Kauffmann, G., et al. 2003a, MNRAS, 341, 33
Kauffmann, G., et al. 2003b, MNRAS, 341, 54
Kennicutt, R. C. 1989, ApJ, 344, 685
Mac Low, M. & Ferrara, A. 1999, ApJ, 513, 142
Pérez-González, P. G., Gil de Paz, A., Zamorano, J., Gallego, J., Alonso-Herrero, A., & Aragón-Salamanca, A. 2003, MNRAS, 338, 525
Paturel, G., Theureau, G., Bottinelli, L., Gouguenheim, L., Coudreau-Durand, N., Hallet, N., & Petit, C. 2003, A&A, 412, 57
Roberts, M. S. 1969, AJ, 74, 859
Sanders, D. B. & Mirabel, I. F. 1996, ARA&A, 34, 749
Shaya, E. J. & Federman, S. R. 1987, ApJ, 319, 76
Strateva, I., et al. 2001, AJ, 122, 1861
Tully, R. B., Verheijen, M. A. W., Pierce, M. J., Huang, J., & Wainscoat, R. J. 1996, AJ, 112, 2471
Verde, L., Oh, S. P., & Jimenez, R. 2002, MNRAS, 336, 541